The Journal of
Chemical Physics

RESEARCH ARTICLE | JULY 14 2023

Inkjet printing on hydrophobic surfaces: Controlled pattern formation using sequential drying FREE

Special Collection: Chemical Physics of Controlled Wettability and Super Surfaces

Paria Naderi ; Benjamin Raskin Sheuten ; Alidad Amirfazli ; Gerd Grau

J. Chem. Phys. 159, 024712 (2023)
https://doi.org/10.1063/5.0149663

The Journal of Chemical Physics | ARTICLE | pubs.aip.org/aip/jcp

Inkjet printing on hydrophobic surfaces: Controlled pattern formation using sequential drying

Cite as: J. Chem. Phys. 159, 024712 (2023); doi: 10.1063/5.0149663
Submitted: 7 March 2023 • Accepted: 19 June 2023 •
Published Online: 14 July 2023

View Online Export Citation CrossMark

Paria Naderi,[1,a)] Benjamin Raskin Sheuten,[2] Alidad Amirfazli,[2] and Gerd Grau[1]

AFFILIATIONS

[1] Department of Electrical Engineering and Computer Science, York University, Toronto, Ontario M3J 1P3, Canada
[2] Department of Mechanical Engineering, York University, Toronto, Ontario M3J 1P3, Canada

Note: This paper is part of the JCP Special Topic on Chemical Physics of Controlled Wettability and Super Surfaces.
[a)] **Author to whom correspondence should be addressed:** panaderi@yorku.ca

ABSTRACT

Inkjet-printed micro-patterns on hydrophobic surfaces have promising applications in the fabrication of microscale devices such as organic thin-film transistors. The low wettability of the surface prevents the inkjet-printed droplets from spreading, connecting to each other, and forming a pattern. Consequently, it is challenging to form micro-patterns on surfaces with low wettability. Here, we propose a sequential printing and drying method to form micro-patterns and control their shape. The first set of droplets is inkjet-printed at a certain spacing and dried. The second set of droplets is printed between these dry anchors on the surface with low wettability. As a result, a stable bridge on the surface with low wettability forms. This printing method is extended to more complicated shapes such as triangles. By implementing an energy minimization technique, a simple model was devised to predict the shape of the inkjet-printed micro-patterns while confirming that their equilibrium shape is mainly governed by surface tension forces. The gradient descent method was utilized with parametric boundaries to emulate droplet pinning and wettability of the anchors and to prevent convergence issues from occurring in the simulations. Finally, the energy minimization based simulations were used to predict the required ink to produce dry lines and triangles with smooth edges.

I. INTRODUCTION

The formation of micro-patterns on surfaces with low wettability, seen in applications such as microelectronic devices and bio-surfaces with cell-based assays, poses a significant challenge.[1,2] Printing techniques such as extrusion and screen printing are not as influenced by substrate wettability compared to other techniques, but their resolution is low.[3,4] To print high-resolution patterns, inkjet printing and gravure printing are used.[5–7] For both of these techniques, ink spreading and pattern formation are influenced by substrate wettability. If a surface has relatively high surface energy, meaning that the ink contact angle is below 90°, lines and other patterns can be printed, but if the contact angle is above 90°, the printed droplets will not spread to merge with each other and form patterns: Printed lines are unstable.[8] The use of hydrophobic films such as Teflon amorphous fluoropolymers (Teflon-AF) as a coating material, device encapsulation, or the gate dielectric in transistors is often inevitable.[9–12] On surfaces with low wettability, adjacent droplets merge and bulge into larger circular drops rather than maintain the printed pattern such as a line or square. Consequently, to deposit functional inks on hydrophobic surfaces, for instance, as conducting electrodes in printed electronics, a common approach is to increase the wettability of the surface using surface modification.[13] For example, to achieve finer thin-film patterning through printing, surfaces with hydrophilic/hydrophobic adjacent regions can be created with plasma treatment. The ink wets the hydrophilic region and is confined by the hydrophobic regions.[14] However, in addition to adding extra manufacturing steps to the process, surface treatment methods such as plasma[15–20] and addition or removal of monolayers[21,22] may alter the surface both chemically and physically,[16] potentially compromising the functionality of the printed micro-patterns.[12]

There are some ways of forming micro-patterns on hydrophobic surfaces without resorting to surface modification. One approach is the chemical modification of the ink, for instance, by using gelation polymers mixed with TiO_2 ink, where the thermal gelation of the ink prevents it from dewetting the hydrophobic surface and helps forming straight lines.[23] This approach requires modifying the ink formulation, which may not always be a viable option. On the other hand, stacked-coin lines have been inkjet-printed on surfaces with high wettability.[24] In this method, the printing stage is heated and the ink is dried immediately after it is deposited on the substrate. Ideally, each droplet is dried before it retracts, and the subsequent droplet is pinned on the previous droplet. When printing stacked-coin lines, the heat from the print stage can cause the solvent to evaporate in the nozzle and hinder droplet jetting due to ink agglomeration.[24] While it helps with pinning the droplets on the surface, it is more applicable to solvents with high boiling point, and due to the high temperature condition, it is not considered as a general method.

Another technique for forming ink patterns on hydrophobic substrates involves printing of the corners of a rectangle and drying them, followed by the deposition of ink between those corners, which is then stretched by the previously dried corner droplets.[25] However, in Ref. 25, the focus was to use the printed pattern as a fully overlapped transistor gate electrode without the need for accurate patterning, low edge roughness, or high resolution. In a similar study leveraging surface tension forces, high-resolution lines were formed by sandwiching a layer of ink between a pre-patterned substrate with printed dots and a cover plate. Bridges were formed between the dots as the ink solvent evaporated.[26] While smooth and well-controlled lines were formed with this method, the process requires careful control over the dewetting process limiting the types of patterns that can be printed. Additionally, the entire surface is initially covered with the ink, which may pose difficulties for complex multilayer devices.

When lines are inkjet-printed on surfaces regardless of wettability, the beginning of the patterns tends to bulge due to Laplace pressure gradient between an already printed larger volume with lower curvature and the newly printed droplet with higher curvature. One way of preventing inkjet-printed lines from bulging at the beginning of the line is to use symmetric printing.[7] With symmetric printing, three-droplet line segments are printed with the middle droplet being printed last. This method prevents the bulging at the beginning of printed patterns[7,27] on surfaces with high wettability; however, it has not yet been explored on surfaces with low wettability. There is a need to understand and control the printed line formation process on hydrophobic surfaces through the development of novel methods.

Simulations can be used to predict printed ink behavior on a surface and prevent waste of material and time while providing better understanding of the pattern formation. Different simulation methods have been employed to predict the formation of micro-patterns, for example, the Navier–Stokes and continuity equations,[28,29] the lattice Boltzmann equation,[30,31] and the energy minimization integral.[32] Among these methods, the energy minimization approach is simple and time-efficient and it can emulate the shape of microdroplets with a high level of accuracy to find a steady-state solution.[33] This method finds the equilibrium state of the droplet by calculating its energy using the surface integral of the applied forces. The minimum energy state for the system represents the equilibrium state.[34,35] Surface Evolver is a popular simulation tool that uses gradient descent method to minimize the energy to study the equilibrium state of droplets by taking into account forces such as surface tension and gravity.[34] The energy is minimized using the gradient descent method, in which each vertex on the surface of the body has an energy and a force that acts on it. The total energy of the surface is a function of the coordinates. The negative of the energy gradient is the force that has a direction from higher to lower energy and moves the vertex in that direction to define the shape of the interface in an iterative process. As such, when running the simulation, the system, through iterations and refinements, moves vertices simultaneously to minimize the surface energy.[34] Gradient descent method is a popular method to find the minimum energy state, but it can have challenges. For example, achieving good convergence by employing the gradient descent method alone is often not possible.[32] One challenge with the energy minimization method is the accurate modeling of the contact angle at the discontinuities between regions of different wettabilities. At these boundaries, the energy minimization integral fails to work. One way of dealing with this problem is replacing the gradient descent method with a direct search method at the boundaries,[32,33] which means using two different methods for the different areas. This approach requires more time and alternating between two algorithms.

To overcome the challenge of printing on hydrophobic surfaces, we have conducted a combination of simulation and experimental work, following the strategy below. To produce micro-patterns on a hydrophobic surface, we inkjet print silver nanoparticle ink on Teflon-AF films. Our method uses printing and drying sequences, where hydrophilic/hydrophobic regions are created on the surface without blanket surface modification. The dried ink from the first printing sequence acts as the hydrophilic region as the high silver nanoparticle content of the ink renders it hydrophilic. The desired pattern is formed in the second step by depositing and drying more ink on the hydrophobic region between pre-printed anchors. In other words, we adopted symmetric printing methodology to inkjet print patterns on hydrophobic surfaces, with a drying step to be inserted into the symmetric printing process to form line segments. Schematics of the sequential printing and drying steps to form micro-patterns are shown in Fig. 1. The edge profile of the line is influenced by the volume of the printed ink. It is crucial to have the ability to anticipate and regulate the required volume of ink for a specific line length, particularly in areas such as microelectronics where pattern dimensions determine electrical performance. Instead of experimental trial-and-error methods to determine accurate micro-pattern dimensions, a computational model was devised based on energy minimization with Surface Evolver to predict the ink volume required to print line segments with different lengths and other patterns such as triangles. The printed patterns are simulated and analyzed with only the contact angle of the ink on the substrate as an input parameter. This allows us to confirm whether surface tension is the main force controlling the equilibrium state of micro-patterns obtained through the sequential print and dry method. The simulation results are used to predict the printed volume necessary to print smooth patterns after drying.

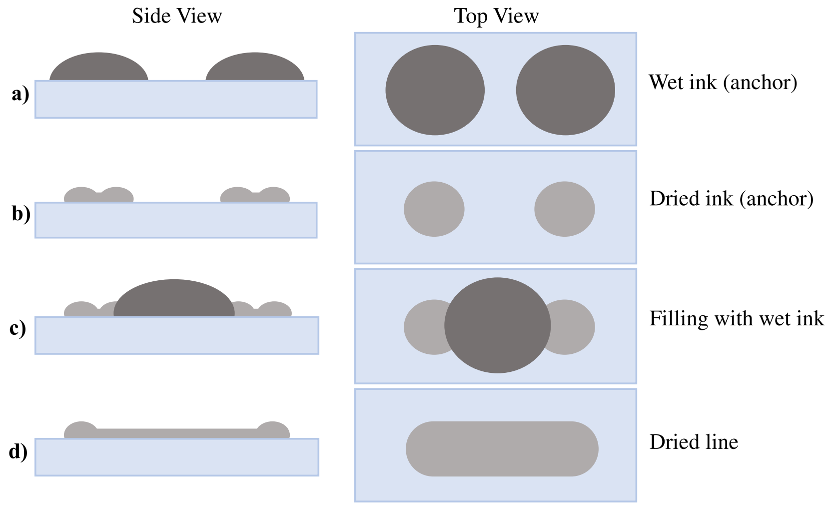

FIG. 1. Schematics of the side and top views of the sequential printing and drying of the micro-patterns with the following steps: (a) Printing the first sequence of droplets, (b) drying droplets, (c) printing the second sequence of droplets, and (d) drying the final pattern.

II. METHODS AND MATERIALS

A. Experimental

1. Materials

Silver nanoparticle ink (ANP DGP 40LT-15C, Advanced Nano Products, Co., Sejong, Korea) was inkjet-printed using a custom-built inkjet-printer with a 60 μm-diameter nozzle (MJ-ATP-01-60-8MX, Microfab Technologies, Inc. Plano, TX). Teflon-AF 1600 (Sigma-Aldrich, Oakville, Canada) was dissolved in Fluorinert FC-40 (Sigma-Aldrich, Oakville, Canada) with a 1.6% concentration.

2. Sample fabrication

The Teflon-AF solution was spin-coated at 500 rpm for 1 min on glass slides and dried at 150 °C for 15 min. Two printing approaches were used for printing lines, i.e., the traditional method (method 1) and the sequential printing and drying method (method 2). In the traditional method, single droplets (volume 0.19 nl) were printed with different spacing, i.e., the drop spacing of the printed single droplets was varied between 10 and 85 μm. In the sequential printing and drying method, first, two anchors each comprising ten droplets (volume 1.9 nl) were printed at different distances from each other (170–260 μm). Next, the printed anchors were dried at 150 °C for 15 min. Finally, different volumes of the ink were printed between the two anchors. For each anchor spacing between 170 and 260 μm, first a minimum volume of ink was printed to connect the anchors. Then, the volume was increased droplet by droplet, to find where a relatively smooth line will form.

3. Characterization

The contact angle of de-ionized (DI) water and silver ink on Teflon-AF and dry silver ink were measured using the sessile drop method (Krüss DSA10, Krüss Scientific, Germany). The contact angle of the silver nanoparticle ink on a Teflon-AF film is 84° ± 2°. Although the surface is not as non-wetting as it is for water with a contact angle of 120° ± 2°, it is still considered as non-wetting in practice. The thickness profiles of the dry droplets were measured using a stylus profilometer (Alpha-Step D-600, KLA-Tencor, USA).

B. Simulations

To model the line pattern formed by the sequential printing and drying method, Surface Evolver was used. The surface in general is defined as a complex of vertices, edges, and facets. A vertex is a point with coordinates. An edge is defined by the head and tail vertices, and each facet is defined by at least three edges. A body is defined by the facets that make up its boundaries. The body initially has an approximate shape (but accurate volume) and later approaches the desired shape defined by the imposed constrains through an iterative evolution. The surface energy is the integral of the forces acting on the surface. For instance, if the force is only surface tension, we can write the energy as

$$E = \iint_{facet} -T\vec{k}\cdot\overrightarrow{dA} = \iint_{facet} -T\cos\theta\cdot dA, \qquad (1)$$

where T is the surface tension, $\vec{k}$ is the surface tension unit vector, A is the area of the facet, and θ is the contact angle of the liquid on the solid surface.

In the present work, the system was defined as two regions having ink contact angles of 84° ± 2° (printing surface) and 0° (anchor region). In the simulation, gravity was ignored since the printed features are in the microscale with a Bond number equal to 4.13×10^{-3}. Silver nanoparticle ink properties are given in Table I. The anchor regions were positioned at a distance of d to each other. Due to geometry limitations in Surface Evolver, anchor regions were assumed to be flat circles flush with the printing surface. In this model, surface properties are applied to a flat substrate surface and the anchor thickness and its variation are not accounted for in the simulation environment as the thickness of the dried anchors is neg-

TABLE I. Silver nanoparticle ink properties.

Surface tension (mN/m)	35
Viscosity (cps)	16.7
Density (g/ml)	1.38
Silver content (wt. %)	31.7
Contact angle (°) on Teflon-AF	84 ± 2
Contact angle (°) on dry silver	12 ± 2

ligible compared with the thickness of the wet the line segment. The radius r of the anchor regions was 39 μm. These circles are the parametric boundaries and are schematically shown in Figs. 2(a) and 2(b).

As detailed in Ref. 34, parametric boundaries are mathematical constrains applied to the geometry of the simulated body and are defined using equations and algorithms. The vertices that are positioned on the boundaries can only move on the 1D boundary paths and they do not participate in the surface minimization process. In the model, half of the vertices were placed on the perimeters of the anchors (fixed), with the other half placed on the top surface of the anchor hemispheres. The anchors were modeled as hemispheres, and the volume of the hemispheres was ignored in the calculation of the total liquid volume because it only represents 2.5% of the volume of a wet droplet. The volume of the anchor hemispheres shown in Fig. 2 does not represent the real volume and it is simply used to hold the initial vertices on its surface. The simulated ink will only see the perimeters of the anchors and is not constrained by any other geometrical boundary. The body was defined as the volume encompassed by edges that connects vertices both on the perimeter and the top surface of the anchor hemispheres. The parametric boundaries were imposed on the edges of the initial body to confine the body (printed ink) to the perimeters of the anchors. This method ensures that the contact angle of 0° can be preserved for anchors. Figure 2(c) shows the initial body confined to the parametric boundaries at the perimeter of the anchors, and Fig. 2(d) shows the same system without parametric boundaries.

Another group of constrains defined in Ref. 34 is that of 2D constraints, which are forces imposing restrictions on the body in two dimensions. The only 2D constraint used in this model is surface tension on the printing surface, see Fig. 2(b). This 2D constraint is the foundation of the model in which the surface tension of the hydrophobic surface is included through Young's equation:

$$\cos(\theta) = \frac{\sigma_{sv} - \sigma_{sl}}{\sigma_{lv}}, \tag{2}$$

where σ_{sv}, σ_{sl}, and σ_{lv} are the solid–vapor, solid–liquid, and liquid–vapor interfacial tensions. This constraint was exerted on the body facet that lies on the surface with low wettability.

III. RESULTS AND DISCUSSION

A. Method 1: Printing continuous lines on a surface with low wettability

Figure 3(a) shows the nozzle and the ejected droplet in the air. Figures 3(b) and 3(c) show single wet and dry droplets on the Teflon-AF surface; the initial volume of both were equal. The dry droplet has

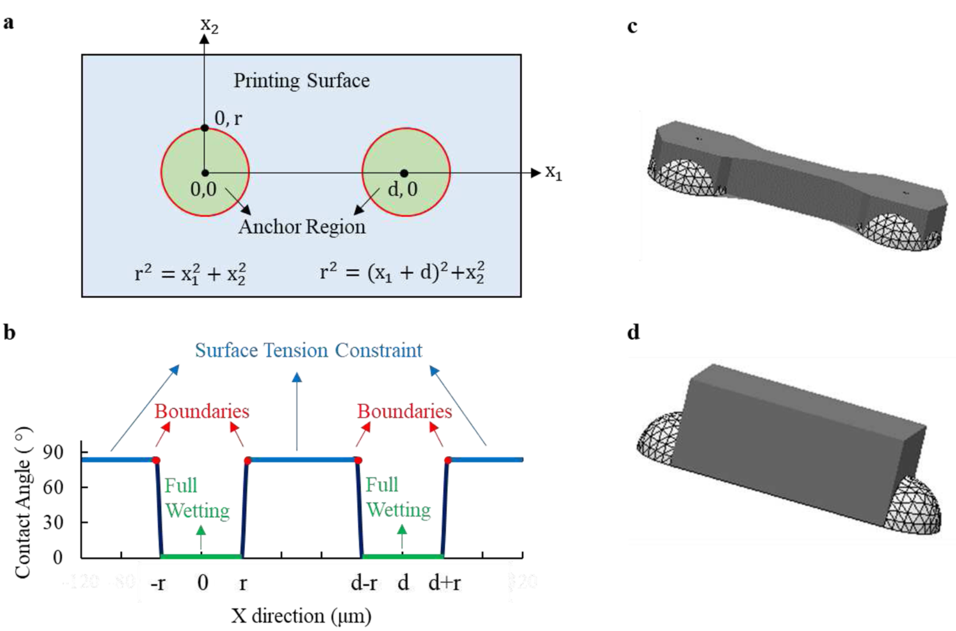

FIG. 2. (a) Top view of the surface view in simulations. The circles represent the previously printed and dried silver drops, i.e., the anchor regions. (b) Local contact angle variation in the x-direction, with boundaries, full wetting, and surface tension constraint regions shown. Initial defined body in Surface Evolver (c) with, and (d) without parametric boundaries imposed on its edges.

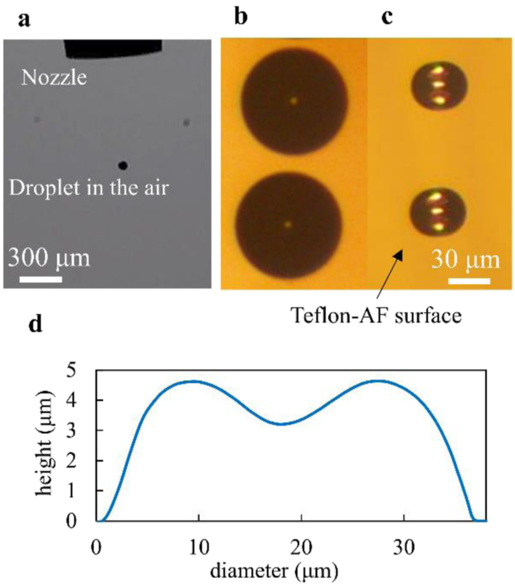

FIG. 3. (a) A 60 μm-diameter inkjet nozzle and an ejected droplet in the air. Inkjet-printed single (b) wet, and (c) dry droplets on Teflon-AF surface. (d) Thickness profile of a single dry droplet.

a radius of 18.6 μm (the diameter of a wet droplet on the Teflon-AF surface is ~71 μm), with an average thickness of 3.4 μm. The thickness profile of a single dry droplet is shown in Fig. 3(d). The dimple in Fig. 3(d) is due to accumulation of material[36,37] on the edges of the droplet due to capillary flow.[38]

Method 1 represents the traditional approach to form lines on a surface. With this method, a series of lines with varied drop spacing was printed with decrements of 5 μm. On a hydrophilic surface, an excessively small drop spacing results in lines that exhibit bulging, and an excessively large drop spacing leads to scalloping and discontinuities in the lines.[7,24] Figure 4(a) depicts a schematics of the inkjet printing process. On a hydrophobic surface, as can be seen in Fig. 4(b), when the drop spacing is small, every few droplets merge, and the number of the merging droplets decreases by increasing the drop spacing. In all panels in Fig. 4(b), the same number of droplets were printed (12). At a drop spacing of 75 μm, individual droplets appear. Beyond a drop spacing of 80 μm, the individual printed droplets no longer merge with one another. This experiment serves to affirm that the Teflon-AF surface exhibits a non-wetting behavior for this silver nanoparticle ink, pointing to the challenge that was discussed earlier to form a continuous line through adjustment of the drop spacing. Changing the volume of printed droplets will not remedy the issue due to same surface thermodynamic principle that governs this phenomenon.

B. Method 2: Sequential printing and drying

Method 2 is our suggested strategy. It was employed to print line segments on a surface with low wettability. Method 2 is a symmetric printing method, where anchors at the two ends of the line segments are printed first, and the middle droplets are printed last. To pin the ink on the surface, the first sequence of droplets was dried before printing the second sequence in the middle. Figure 5 shows the process. First, two anchors with a distance of 200 μm were printed and dried [Fig. 5(a)]. Each wet anchor has the volume of 1.93 nl (ten single printed droplets). Subsequently, ink volumes of 1.8–6.4 nl were printed between anchor regions and dried [see Figs. 5(b)–5(e)]. It can be observed from Fig. 5 that varying the volume of the printed droplets in between the anchors changes the shape of the line segments. As the ink volume is gradually increased, the width of the line segments increases accordingly. When the volume of the printed droplets is insufficient, the connection is hardly formed after drying [Fig. 5(b)]. As the volume is increased, the connection widens, but it remains thinner than the anchor diameter [Fig. 5(c)]. At a specific volume for a given line segment length, the dry linewidth approaches the anchor diameter [Fig. 5(d)], resulting in a smooth line after drying. However, further increasing the ink volume results in a line segment width larger than the anchor diameter [Fig. 5(e)], which is generally not desirable. Considering above, the strategy suggested in this study works for printing lines. Longer lines can be generated by simply repeating this process; even corners can be formed by positioning the next dry anchor not along the initial line but at a desired orientation.

C. Simulating the sequential printing and drying process

To minimize experimentation to produce printed lines with different characteristics and explore patterns other than a line, the wet patterns were simulated. Figures 6(a) and 6(b) show the experimental and simulated line segments before drying with the anchor distance of 200 μm for different ink volumes of 1.2, 3.2, and 5.0 nl. Figure 6(c) shows the graph of the midpoint for wet linewidth vs the printed volume for the same anchor distance; the objective is to attain a smooth line, so the width of the midpoint for the line was used as the point of comparison, the midpoint of the line was selected since it shows the most deviation from a straight line that is the goal of the work. Figure 6 shows an excellent agreement between experiment and simulation with an average error of 1.1%.

The distance between the two anchors was varied in both experiments and simulations. The results for the anchor distances of 170, 230, and 260 μm are shown in Fig. 7. Again, the inkjet-printed experimental and simulated data are very close to each other and follow the same trend. The optical images of the inkjet-printed and simulated line segments for the volume of 5.6 nl for different lengths are also presented in Fig. 7.

Parametric boundaries were used on the perimeter of the anchors where the wettability abruptly changes from one region to the other, to avoid discontinuities in the gradient descent method. Defining parametric boundaries at the location of discontinuities allows us to remove the discontinuous coordinates from the energy minimization integral by fixing them in place. The implementation of surface tension via the contact angle ($T\vec{k} \cdot \overrightarrow{dA} = T\cos\theta \cdot dA$) as a 2D constraint leads to simulation results that fit the results obtained from printed patterns. As confirmed by this model, the formation of microdroplets with the sequential drying method is mainly governed by the surface energy of the substrate. Factors such as gravity,

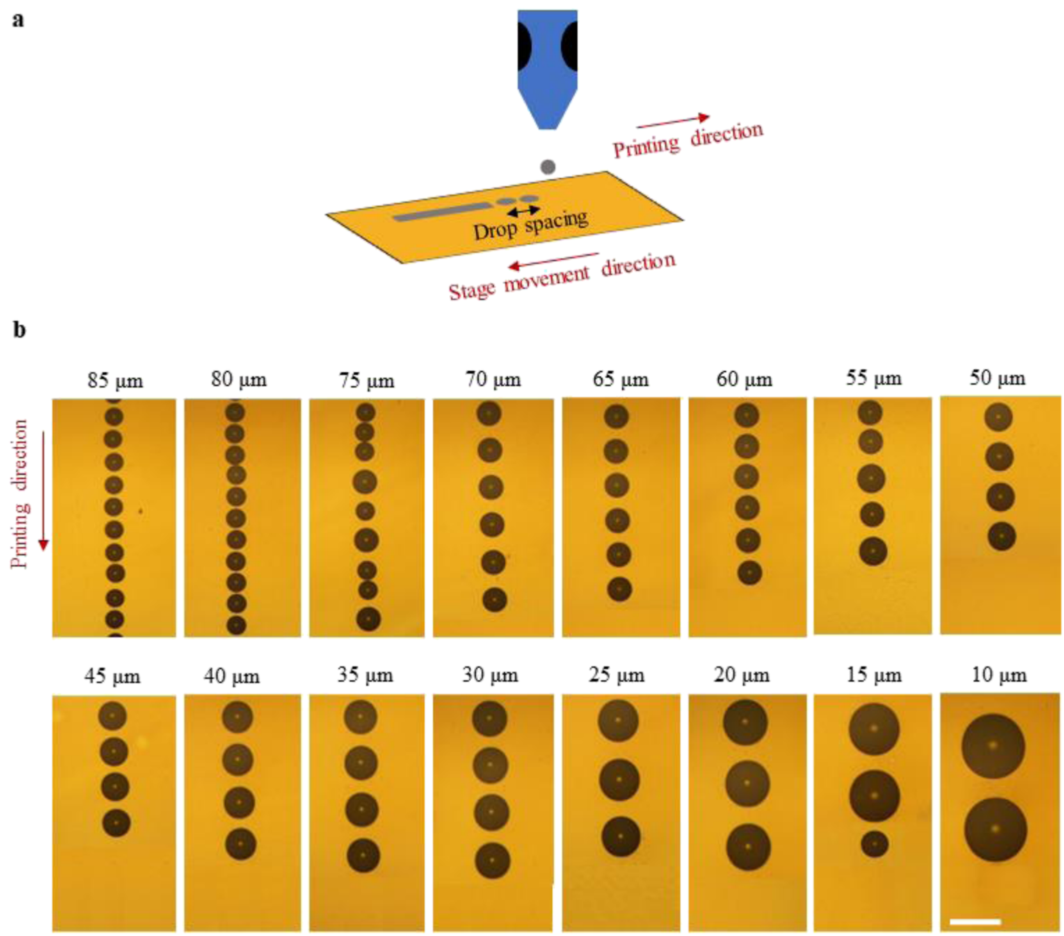

FIG. 4. (a) Schematic of the inkjet printing process. (b) Inkjet-printed silver nanoparticle lines with different drop spacing on the Teflon-AF surface. The drop spacing for each image is shown on top of the image. The scale bar represents 200 μm. The volume of a drop in the air is 0.19 nl.

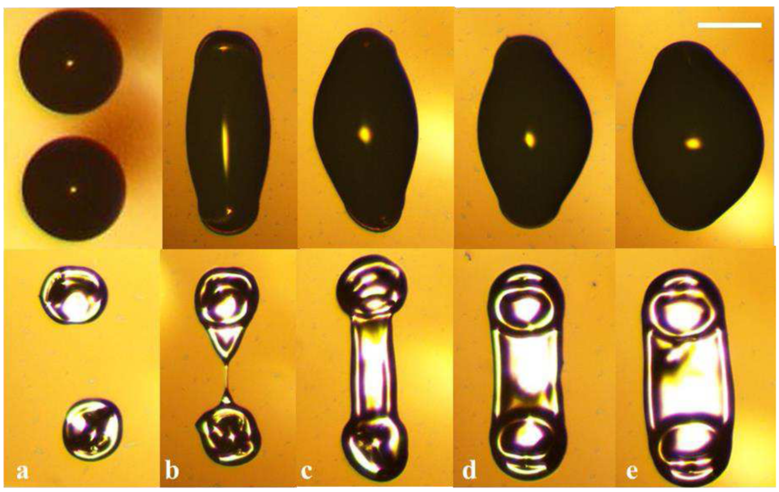

FIG. 5. Optical images of line segments printed with method 2 in the wet (top row) and dry (bottom row) state. (a) Step one to form the anchor regions. Subsequently printed ink between anchor regions with ink volume of (b) 1.8 nl, (c) 3.6 nl, (d) 5 nl, and (e) 6.4 nl. The scale bar represents 100 μm. The droplet separation distance is 200 μm. In each column, the top row shows the line segments before drying, and the bottom row shows the same line segments after drying (at 150 °C for 15 min).

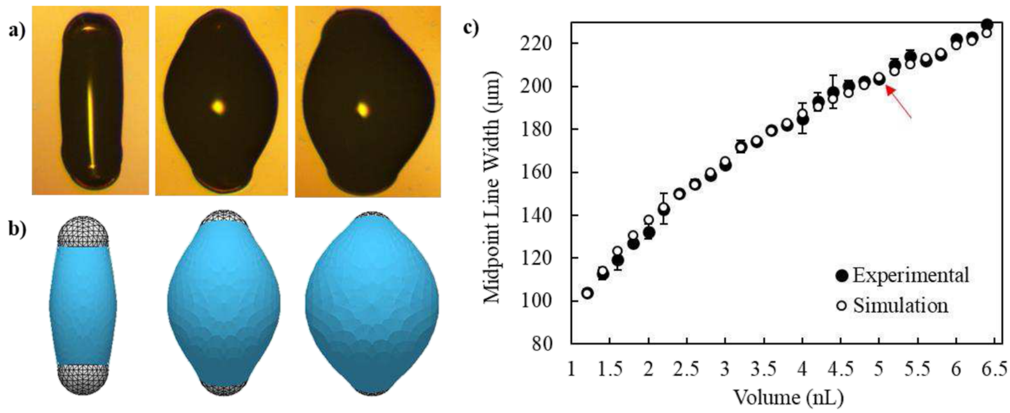

FIG. 6. Experimental printed (a) and simulated line segments (b) with the anchor distance of 200 μm for volumes of 1.2, 3.2, and 5.0 nl from left to right. The scale bar is 100 μm. (c) Graph of wet midpoint linewidth vs printed ink volume showing good agreement between experiment and simulation. The red arrow marks the volume of ink resulting in a final smooth dry line segment.

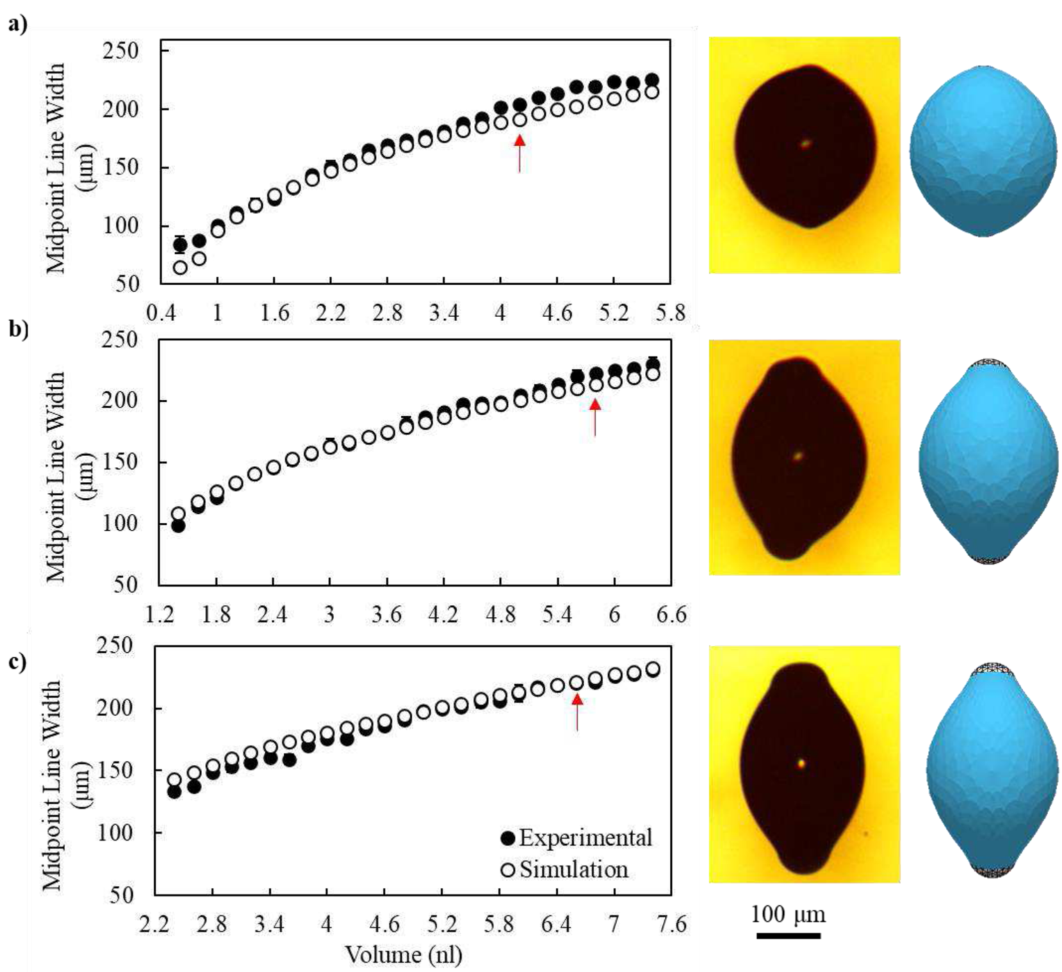

FIG. 7. From left to right, graphs of the midpoint linewidth vs printed ink volume, top view images of printed and simulated line segments for an anchor distance of (a) 170 μm, (b) 230 μm, and (c) 260 μm. Red arrows point to a volume that results in a straight dry line in each case. The images of line segment are all for the volume of 5.6 nl.

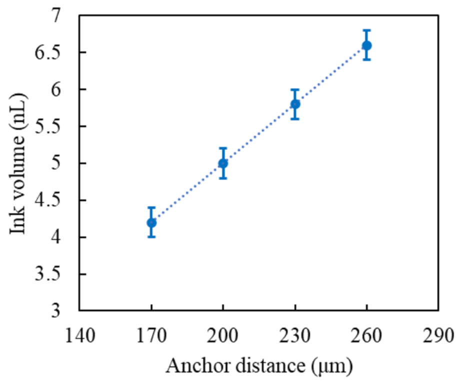

FIG. 8. The ink volume needed to produce a smooth line segment vs line segment length. The graph shows a linear relationship between the Vol_{wet} and anchor distance and its linear fit. The slope of the linear fit is 2.7×10^4 μm^2 (with y-intercept, standard error and R^2 being equal to -0.3 nl, 5.2×10^{-18} nl and 1.00, respectively). The error bars show error margin of one droplet (0.2 nl).

pinning, and drop impact do not significantly influence the equilibrium state of micro-patterns obtained through the sequential drying method as these phenomena are not included in the model.

Understanding the surface tension forces that lead to the minimal energy state allows us to understand the final ink shape. Without the anchors, the wet ink makes a contact angle of ~90° with the surface and becomes a hemisphere instead of a line to minimize surface energy. As there is no pinning, no stable line can be formed. Increasing ink volume only adds to the hemisphere's radius. The anchors add two areas where pinning of contact line occurs, allowing for the formation of a line. Due to the high surface energy of the dried silver anchors, surface energy is minimized when the wet ink fully wets the anchors. This constraint allows the formation of a line rather than a hemisphere. The positioning of the ink exactly in the midpoint of the anchors leads them to be equally covered by wet ink. Therefore, a bridge of ink forms between the anchors, which increases in width with increasing ink volume as seen in Fig. 5.

If we plot the ink volume vs the anchor distance, which leads to a straight line with smooth edges (From Figs. 6 and 7), a line with constant slope can be found (see Fig. 8); the error bars show an error margin of one droplet (0.2 nl). Such behavior suggests two possibilities. First, it can mean that a print factor (PF) exists correlating the required printed volume to the anchor distance (d), i.e.,

$$Vol_{wet} = d \times PF. \tag{3}$$

The interesting point about PF is that it does not need to be calculated for each case; rather, it can be derived from a single experiment with a specific line length and be extended to other line lengths.

The second implication of PF is that it indicates that there should be a relationship between the volume of the ink and the width of line that remains after the ink has been dried. This is very interesting as it means the simulation alone can be used to potentially predict the resultant printed features. This will be further explained below, but before that in Fig. 9 we show that this method of printing can be used for printing other features such as triangles using three-anchor patterns. Using method 2, we printed equilateral triangles and compared the results with simulations. The top view optical images of the inkjet-printed experimental and simulated triangles and the graphs of the image area vs printed ink volume are shown in Fig. 9.

To demonstrate the second implication of Fig. 8, we need to consider the drying process of the ink, i.e., the removal of the solvent and having only the solute (silver nanoparticles) left behind. The fact that we can predict the final ink pattern only considering surface energy minimization means that the dynamics of the drying process do not significantly affect the final equilibrium state. The drying of the ink where the contact line recedes and the final line shape achieved is much slower, i.e., in the order of minutes compared to

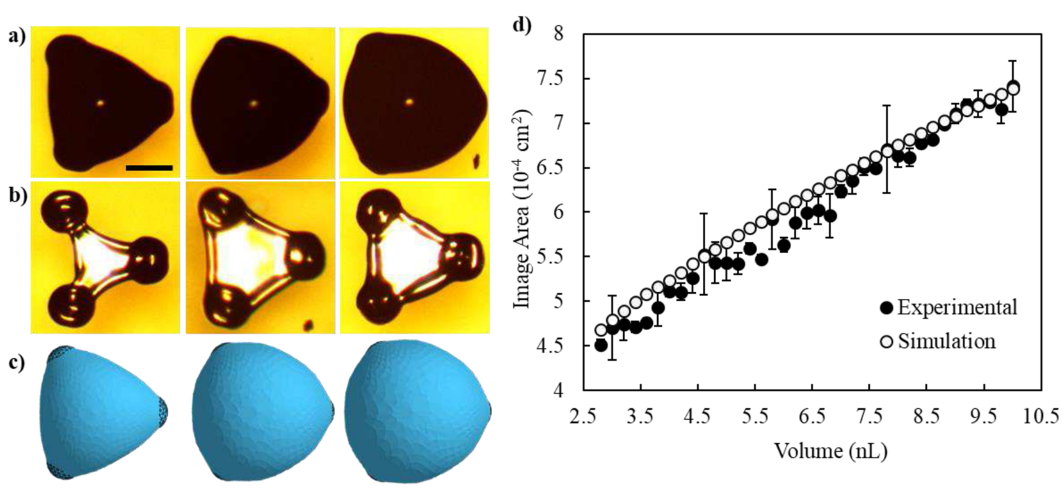

FIG. 9. Optical images of (a) wet and (b) dry printed, and (c) simulated equilateral triangles (side dimension = 200 μm), with ink volumes of 5.2, 8.8, and 9.8 nl from left to right. The scale bar represents 100 μm. (d) The simulated and inkjet-printed image area vs ink volume with a percentage error of 2.9%.

spreading—under a second (see video of the drying process of a line segment with an anchor distance of 200 μm while stage temperature increases from 22 to 150 °C the in the supplementary material). The drying process will determine the feature dimension, which is of great importance in microelectronics since it affects electrical properties. The simulations can be used to predict the dry shape and, in particular, the printed volume required to form straight smooth features on hydrophobic surfaces. The linewidth vs volume for all the four tested anchor distances in Figs. 6 and 7 can be fit to a square root function,

$$w = A\sqrt{V}, \tag{4}$$

where w is the linewidth, V is the printed volume or V_{wet}, and A is a fitting parameter. There are two distinct phases in the drying process of a droplet (or a pattern in general) on a surface with low contact angle hysteresis. The schematic drawing in Fig. 9(a) shows the drying process of a droplet, starting from an initial wet droplet with the diameter of w_{wet}. In the first phase, as the droplet dries, the contact line recedes without being pinned to the surface due to the low wettability of the surface, while the contact angle stays fixed. Therefore, the droplet maintains the shape of a spherical cap. The volume of a spherical cap is proportional to the cube of its radius (r^3). The onset of the second phase is when the droplet becomes pinned. The simulations are based on energy minimization of the liquid surface and hold only for phase one. In phase one, the droplet is regarded as a spherical cap, so for the volume ratio between the pinned and wet state, we will have the following value based on the measured drop radii for this ink on Teflon-AF:

$$\text{vol\%} = \frac{V_{pin}}{V_{wet}} = \left(\frac{r_{pin}}{r_{wet}}\right)^3 = \left(\frac{18.6}{35.5}\right)^3 = 14.38\%. \tag{5}$$

In phase two, the concentration and viscosity of the ink have increased sufficiently to inhibit the contact line from further movement, and the droplet contact angle starts to reduce (constant contact angle mode of drop evaporation[36]). When pinning starts, the cord length (or contact length) in Fig. 10(a) is w_{pin} (which is assumed to be equal to w_{dry}). Substituting w_{pin} in Eq. (4) leads to a value for V_{pin} and, using the volume ratio in Eq. (5), V_{wet} can be calculated. We assume that the same relationships and assumptions hold for lines and other features, too, which were validated for lines and triangles. The V_{wet} value that results in smooth line segments (linewidth equal to anchor diameter) was measured for four different anchor distances. Figures 10(b)–10(e) show the wet and smooth dry line segments for anchor distances of 170, 200, 230, and 260 μm, respectively. The plot in Fig. 10(f) shows values for the printed volume needed to create smooth line segments vs the anchor distance for the experimental and simulation results. The values predicted from the simulation are close to the experimental results with an average absolute error of 10.7%. The same method was used to predict the area of triangles printed with different ink volumes and shows a good match with experiment with an average absolute error of 22.2%. The larger error for triangles is likely due to

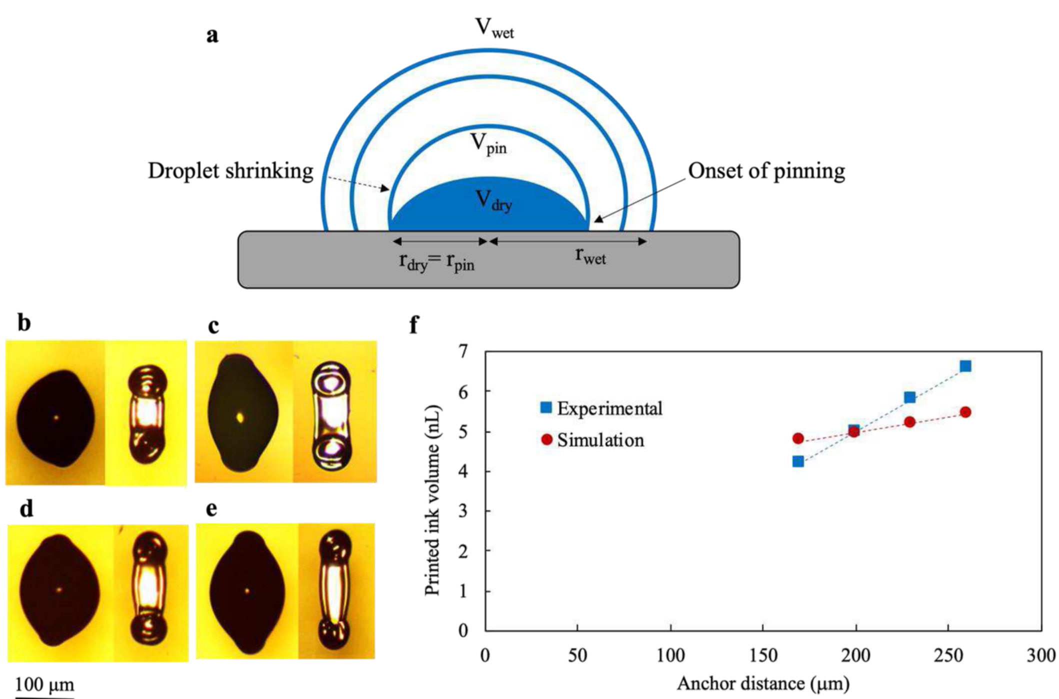

FIG. 10. (a) The drying process of a droplet, starting from an initial wet droplet with the diameter of w_{wet} until its diameter reaches w_{pin} in phase one. In phase two, the contact line is pinned as the drop volume is reduced to V_{dry}. Images of smooth line segments in the wet and dry state for anchor distances of (b) 170, (c) 200, (d) 230, and (e) 260 mm, respectively. (f) The printed volume needed to print a smooth dry line segment vs the anchor distance for the experimental and simulation results.

their more complicated shape having three anchors and three edges with complications arising from their pinning process.

IV. CONCLUSION

A new printing method is shown to form micro-patterns on surfaces with low wettability that does not require surface modification. A model based on energy minimization predicts the shape of the inkjet-printed micro-patterns with good accuracy and only the contact angle of the ink on the surface as the input, confirming that the formation and equilibrium state of these micro-patterns are mainly governed by surface tension forces. Line segments with different length were printed and simulated. Both the experimental and simulation methods are extended to more complicated shapes such as triangles. Moreover, the energy minimization based simulations were used to predict the required printed ink to produce smooth dry features, which show good agreement with experimental results.

SUPPLEMENTARY MATERIAL

We have added a video of drying line segments printed with an anchor distance of 200 μm as supplementary material. The stage temperature increases from 22 to 150 °C in the video. During the drying of the ink, the contact line recedes and the width of the line segments decreases.

ACKNOWLEDGMENTS

We acknowledge the support of the Natural Sciences and Engineering Research Council of Canada (NSERC), funding reference number STPGP 521480-18. EU H2020-MSCA-RISE-778104-ThermaSMART is thanked for internship opportunity for Ben Raskin Sheuten. We would also like to thank Professor Kenneth Brakke from the Department of Mathematics at Susquehanna University for his generous help with the Surface Evolver simulations. Profilometry measurements were done at York University Microfabrication Facility (YMF).

AUTHOR DECLARATIONS

Conflict of Interest

The authors have no conflicts to disclose.

Author Contributions

Paria Naderi: Data curation (equal); Formal analysis (equal); Methodology (equal); Validation (equal); Writing – original draft (equal); Writing – review & editing (equal). **Benjamin Raskin Sheuten**: Data curation (equal); Formal analysis (equal); Investigation (equal). **Alidad Amirfazli**: Conceptualization (equal); Formal analysis (equal); Funding acquisition (equal); Methodology (equal); Supervision (equal); Writing – review & editing (equal). **Gerd Grau**: Conceptualization (equal); Funding acquisition (equal); Methodology (equal); Project administration (equal); Supervision (equal); Writing – review & editing (equal).

DATA AVAILABILITY

The data that support the findings of this study are available from the corresponding author upon reasonable request.

REFERENCES

[1] K.-H. Shin, H. A. D. Nguyen, J. Park, D. Shin, and D. Lee, "Roll-to-roll gravure printing of thick-film silver electrode micropatterns for flexible printed circuit board," J. Coat. Technol. Res. **14**(1), 95–106 (2017).

[2] D. Falconnet, G. Csucs, H. Michelle Grandin, and M. Textor, "Surface engineering approaches to micropattern surfaces for cell-based assays," Biomaterials **27**(16), 3044–3063 (2006).

[3] M. K. Idris, P. Naderi, G. W. Melenka, and G. Grau, "Damage location sensing in carbon fiber composites using extrusion printed electronics," Funct. Compos. Struct. **3**(4), 045001 (2021).

[4] Y. Kim, B. Lee, S. Yang, I. Byun, I. Jeong, and S. M. Cho, "Use of copper ink for fabricating conductive electrodes and RFID antenna tags by screen printing," Curr. Appl. Phys. **12**(2), 473–478 (2012).

[5] L. Nayak, S. Mohanty, S. K. Nayak, and A. Ramadoss, "A review on inkjet printing of nanoparticle inks for flexible electronics," J. Mater. Chem. C **7**(29), 8771–8795 (2019).

[6] G. Grau, J. Cen, H. Kang, R. Kitsomboonloha, W. J. Scheideler, and V. Subramanian, "Gravure-printed electronics: Recent progress in tooling development, understanding of printing physics, and realization of printed devices," Flexible Printed Electron. **1**, 023002 (2016).

[7] R. Abunahla, M. S. Rahman, P. Naderi, and G. Grau, "Improved inkjet-printed pattern fidelity: Suppressing bulges by segmented and symmetric drop placement," J. Micro Nano-Manuf. **8**(3), 031001 (2020).

[8] J. Stringer and B. Derby, "Formation and stability of lines produced by inkjet printing," Langmuir **26**(12), 10365–10372 (2010).

[9] W. C. Shin, S. Seo, and B. J. Cho, "Highly air-stable electrical performance of graphene field effect transistors by interface engineering with amorphous fluoropolymer," Appl. Phys. Lett. **98**(15), 153505 (2011).

[10] J. Lefebvre, J. Ding, Z. Li, F. Cheng, N. Du, and P. R. L. Malenfant, "Hysteresis free carbon nanotube thin film transistors comprising hydrophobic dielectrics," Appl. Phys. Lett. **107**(24), 243301 (2015).

[11] B. Ameduri, "Fluoropolymers: The right material for the right applications," Chem. –Eur. J. **24**(71), 18830–18841 (2018).

[12] P. Naderi and G. Grau, "Organic thin-film transistors with inkjet-printed electrodes on hydrophobic Teflon-AF gate dielectric with reversible surface properties," Org. Electron. **108**, 106612 (2022).

[13] J. Wu, R. C. Roberts, N. C. Tien, and D. Li, "Inkjet printed silver patterning on PDMS to fabricate microelectrodes for microfluidic sensing," in *Proceedings of IEEE Sensors* (IEEE, 2014), pp. 1100–1103.

[14] H. Sirringhaus, T. Kawase, R. H. Friend, T. Shimoda, M. Inbasekaran, W. Wu, and E. P. Woo, "High-resolution inkjet printing of all-polymer transistor circuits," Science **290**(5499), 2123–2126 (2000).

[15] S. Zanini, R. Barni, R. D. Pergola, and C. Riccardi, "Modification of the PTFE wettability by oxygen plasma treatments: Influence of the operating parameters and investigation of the ageing behaviour," J. Phys. D: Appl. Phys. **47**(32), 325202 (2014).

[16] N. Sprang, D. Theirich, and J. Engemann, "Surface modification of fluoropolymers by microwave plasmas: FTIR investigations," Surf. Coat. Technol. **98**(1–3), 865–871 (1998).

[17] D. J. Wilson, R. L. Williams, and R. C. Pond, "Plasma modification of PTFE surfaces. Part I: Surfaces immediately following plasma treatment," Surf. Interface Anal. **31**(5), 385–396 (2001).

[18] A. Vesel, M. Mozetic, and A. Zalar, "XPS characterization of PTFE after treatment with RF oxygen and nitrogen plasma," Surf. Interface Anal. **40**(3–4), 661–663 (2008).

[19] N. Vandencasteele, D. Merche, and F. Reniers, "XPS and contact angle study of N_2 and O_2 plasma-modified PTFE, PVDF and PVF surfaces," Surf. Interface Anal. **38**(4), 526–530 (2006).

[20]C.-C. Cho, R. M. Wallace, and L. A. Files-Sesler, "Patterning and etching of amorphous teflon films," J. Electron. Mater. **23**(8), 827–830 (1994).
[21]Y. Ito, M. Heydari, A. Hashimoto, T. Konno, A. Hirasawa, S. Hori, K. Kurita, and A. Nakajima, "The movement of a water droplet on a gradient surface prepared by photodegradation," Langmuir **23**(4), 1845–1850 (2006).
[22]S.-H. Choi and B.-m. Zhang Newby, "Micrometer-scaled gradient surfaces generated using contact printing of octadecyltrichlorosilane," Langmuir **19**(18), 7427–7435 (2003).
[23]A. M. J. van den Berg, A. W. M. de Laat, P. J. Smith, J. Perelaer, and U. S. Schubert, "Geometric control of inkjet printed features using a gelating polymer," J. Mater. Chem. **17**(7), 677–683 (2007).
[24]D. Soltman and V. Subramanian, "Inkjet-printed line morphologies and temperature control of the coffee ring effect," Langmuir **24**(5), 2224–2231 (2008).
[25]A. Pierre, M. Sadeghi, M. M. Payne, A. Facchetti, J. E. Anthony, and A. C. Arias, "All-printed flexible organic transistors enabled by surface tension-guided blade coating," Adv. Mater. **26**, 5722–5727 (2014).
[26]S. Chen, M. Su, C. Zhang, M. Gao, B. Bao, Q. Yang, B. Su, Y. Song, S. Chen, M. Su, C. Zhang, M. Gao, B. Bao, Q. Yang, B. Su, and Y. Song, "Fabrication of nanoscale circuits on inkjet-printing patterned substrates," Adv. Mater. **27**(26), 3928–3933 (2015).
[27]F. Pervin Brishty and G. Grau, "Machine vision methodology for inkjet printing drop sequence generation and validation," Flexible Printed Electron. **6**(3), 035009 (2021).
[28]M. Sussman, P. Smereka, and S. Osher, "A level set approach for computing solutions to incompressible two-phase flow," J. Comput. Phys. **114**(1), 146–159 (1994).
[29]D. Jacqmin, "Calculation of two-phase Navier–Stokes flows using phase-field modeling," J. Comput. Phys. **155**(1), 96–127 (1999).
[30]J. Léopoldès, A. Dupuis, D. G. Bucknall, and J. M. Yeomans, "Jetting micron-scale droplets onto chemically heterogeneous surfaces," Langmuir **19**(23), 9818–9822 (2003).
[31]H. Kusumaatmaja and J. M. Yeomans, "Modeling contact angle hysteresis on chemically patterned and superhydrophobic surfaces," Langmuir **23**(11), 6019–6032 (2007).
[32]H. Matsui, Y. Noda, and T. Hasegawa, "Hybrid energy-minimization simulation of equilibrium droplet shapes on hydrophilic/hydrophobic patterned surfaces," Langmuir **28**(44), 15450–15453 (2012).
[33]Y. Noda, H. Matsui, H. Minemawari, T. Yamada, and T. Hasegawa, "Observation and simulation of microdroplet shapes on surface-energy-patterned substrates: Contact line engineering for printed electronics," J. Appl. Phys. **114**(4), 044905 (2013).
[34]K. A. Brakke, Surface Evolver Manual, 2013.
[35]K. A. Brakke, "The surface evolver," Exp. Math. **1**(2), 141–165 (1992).
[36]J. Xu, Z. Wang, and H. C. W. Chu, "Unidirectional drying of a suspension of diffusiophoretic colloids under gravity," RSC Adv. **13**(14), 9247–9259 (2023).
[37]G. Gerber, M. Bensouda, D. A. Weitz, and P. Coussot, "Self-limited accumulation of colloids in porous media," Phys. Rev. Lett. **123**(15), 158005 (2019).
[38]M. Layani, M. Gruchko, O. Milo, I. Balberg, D. Azulay, and S. Magdassi, "Transparent conductive coatings by printing coffee ring arrays obtained at room temperature," ACS Nano **3**(11), 3537–3542 (2009).